Role of Normal Layers in Penetration Depth Determinations of the Pairing State in High-T_c Superconductors

Richard A. Klemm
Materials Science Division, Argonne National Laboratory, Argonne, Illinois 60439

Samuel H. Liu
Solid State Division, Oak Ridge National Laboratory, Oak Ridge, Tennessee 37831-6032
(Received 9 June 1994; revised manuscript received 24 October 1994)

We calculate the penetration depth $\lambda(T)$ for a model of the high-T_c superconductors based upon proximity coupling between one superconducting (S) and one normal (N) layer per unit cell. The linear, low-T region of the $\lambda_{ab}(T)$ data of Bonn *et al.* on $YBa_2Cu_3O_{7-\delta}$ is fitted *quantitatively* for both s-wave and $d_{x^2-y^2}$ order parameters. However, these fitted models give very *different* predictions for $\lambda_c(T)$, which may serve as a new test for the order parameter, or at least for the role of N layers.

PACS numbers: 74.25.Ha, 74.72.Bk, 74.80.Dm

Recently, there has been a raging controversy regarding the orbital symmetry of the order parameter (OP) in high-T_c superconductors. Most of the experiments have been performed on $YBa_2Cu_3O_{7-\delta}$ (YBCO) or on $Bi_2Sr_2CaCu_2O_{8+\delta}$ (BSCCO). Low-temperature T photoemission experiments [1] on BSCCO and corner SQUID and Josephson junction experiments [2] on YBCO were interpreted in terms of $\Delta_{\mathbf{k}}(T)$ having the $d_{x^2-y^2}$ form, $\Delta_d(T)\cos 2\theta_{\mathbf{k}}$. For a two-dimensional superconductor without normal layers, such a gap function would exhibit line nodes at $k_x = \pm k_y$ on the cylindrical Fermi surface [3]. On the other hand, Josephson junction tunneling along the c axis [4] and across grain boundaries [5], plus $\mathbf{H} \perp \hat{\mathbf{c}}$ torque measurements [6] on YBCO, were consistent with s-wave symmetry, $\Delta_{\mathbf{k}}(T) = \Delta_s(T)$. Of these, [5] and [6] were inconsistent with any OP anisotropy within the CuO_2 layers exceeding 25%. More confusing are the penetration depth λ measurements [7–10] on YBCO, which yielded low-T $\lambda_{ab}(T)$ curves which were linear [7], two-gap-like [8], and quadratic [9,10]. While the experiment of [8] was interpreted in terms of an s-wave OP, that of [7] was interpreted in terms of a d-wave OP. Meanwhile, measurements of λ and the surface impedance in $Nd_{1.85}Ce_{0.15}CuO_4$ (NCCO) were quantitatively in agreement with BCS theory [11].

In view of the above discrepancies, it would be interesting to see if a single theory could be made to be consistent with all of the above results. One of us (R. K.) [12] argued recently that the corner SQUID and Josephson junction experiment could be consistent with s-wave OP symmetry, due to a corner effect. In addition, we [13] showed that the surface states present in this model can explain both the apparent gap anisotropy observed in photoemission experiments [1] and the variety of tunneling data obtained from break junction, point contact, and junction tunneling experiments on YBCO and BSCCO. In this Letter, we shall show that the linear low-T $\lambda_{ab}(T)$ behavior observed in [7] can be fitted *quantitatively* with *either* s- or d-wave superconductivity, *provided* that one properly takes account of the normal CuO chain layers. The same model could be used to fit the other data of [8–10]. Since NCCO has only one layer per unit cell, a simplification of our s-wave model is completely consistent with the observed BCS $\lambda(T)$ behavior [11]. In addition, we calculated $\lambda_c(T)$ for our model with both s- and d-wave pairing, and show that a simultaneous measurement of $\lambda_{ab}(T)$ and $\lambda_c(T)$ can distinguish between these models.

We assume two conducting layers per unit cell, in which the quasiparticle propagate freely. The superconducting pairing only takes place within the superconducting (S) (CuO_2) layers, and the other conducting layers are nominally normal (N). The effective masses m_1 and m_2 in the S and N layers differ by the factor $\beta = m_1/m_2 \approx 5$, to account for two strongly correlated S layers per unit cell. Between the S and N layers, the quasiparticles hop with matrix elements J_1 and J_2 across the insulating barriers of thickness d and $d' = s - d$, respectively. Choosing units in which $\hbar = c = k_B = 1$, the model Hamiltonian is $H = H_0 + V$, where

$$H_0 = \int d^2r \sum_{\sigma} \sum_{j=1}^{\infty} \Bigg(\sum_{n=1}^{2} \psi^{\dagger}_{jn\sigma}(\mathbf{r})[(-i\nabla + e\mathbf{A})^2/2m_n - \mu_n]\psi_{jn\sigma}(\mathbf{r}) + [J_1\psi^{\dagger}_{j1\sigma}(\mathbf{r})\psi_{j2\sigma}(\mathbf{r})\exp(i\phi^{j2}_{j1}) + J_2\psi^{\dagger}_{j2\sigma}(\mathbf{r})\psi^{\dagger}_{j+1,1\sigma}(\mathbf{r})\exp(i\phi^{j+1,1}_{j2}) + \text{H.c.}] \Bigg), \tag{1}$$

$$\phi^{j'n'}_{jn}(\mathbf{r}) = -e \int_{js+(n-1)d}^{j's+(n'-1)d} A_z(\mathbf{r})\, dz\,, \tag{2}$$

0031-9007/95/74(12)/2343(4)$06.00

$\mu_n = k_{F\|}^2/2m_n$ is the chemical potential of the nth layer per unit cell, e is the quasiparticle charge, σ is the spin index, and j indexes the unit cells. This form for μ_n conserves $\mathbf{k} = (k_x, k_y)$ at the Fermi energy $E_F \equiv \mu_1$ before and after interlayer tunneling. The vector potential $A(\mathbf{r}) = (\mathbf{A}, A_z)$ is introduced in gauge-invariant form, assuming the semiclassical approximation, and we have neglected the Zeeman energy splittings. The interaction term

$$V = -\frac{1}{2}\int \frac{d^2\mathbf{k}}{(2\pi)^2}\int \frac{d^2\mathbf{k}'}{(2\pi)^2}\sum_{j\sigma}\lambda_{\mathbf{k},\mathbf{k}'}\psi^\dagger_{j1\sigma}(\mathbf{k}')\psi^\dagger_{j1,-\sigma}(-\mathbf{k}')\psi_{j1,-\sigma}(-\mathbf{k})\psi_{j1\sigma}(\mathbf{k}) \tag{3}$$

forms either s-wave pairs with $\lambda_{\mathbf{k},\mathbf{k}'} = \lambda_0$ or $d_{x^2-y^2}$ pairs with $\lambda_{\mathbf{k},\mathbf{k}'} = 2\lambda_0\cos2\theta_{\mathbf{k}}\cos2\theta_{\mathbf{k}'}$ within the S ($n = 1$) layers for energies within $\omega_\|$ of E_F. This s-wave model has been studied [14–16], although the anisotropy of $\lambda(T)$ obtained in [16] was only qualitative.

We may Fourier transform to momentum space, using

$$\psi_{jn\sigma}(\mathbf{r}) = \mathcal{V}^{-1/2}\sum_k \exp(i\{\mathbf{k}\cdot\mathbf{r} + k_z[js + (n-1)d] \mp \phi(k_z)/2\})\psi_{n\sigma}(k), \tag{4}$$

where $k = (\mathbf{k}, k_z)$, the upper (lower) sign refers to $n = 1$ (2), $\mathcal{V}$ is the sample volume, and $\phi(k_z)$ is given by

$$\tan\phi(k_z) = \frac{J_2\sin(k_z d') - J_1\sin(k_z d)}{J_2\cos(k_z d') + J_1\cos(k_z d)}. \tag{5}$$

The quasiparticle Green functions are then defined in the usual temperature-ordered way,

$$G_{nn'}(k, \tau - \tau') = -\langle T[\psi_{n\sigma}(k,\tau)\psi^\dagger_{n'\sigma}(k,\tau')]\rangle,$$
$$F_{nn'}(k, \tau - \tau') = \langle T[\psi_{n\sigma}(k,\tau)\psi_{n',-\sigma}(-k,\tau')]\rangle, \tag{6}$$

etc., where $\langle\cdots\rangle$ represents the thermodynamic average, and the spin indices have been suppressed. The OP $\Delta_{\mathbf{k}}$ for both the s-wave and $d_{x^2-y^2}$ cases is given by

$$\Delta_{\mathbf{k}'} = T\sum_{|\omega|\le\omega_\|}\int \frac{d^3k}{(2\pi)^3}\lambda_{\mathbf{k},\mathbf{k}'}F_{11}(k,\omega), \tag{7}$$

where ω represents the Matsubara frequencies and $\int d^3k \equiv \int d^2\mathbf{k}\int_{-\pi/s}^{\pi/s} dk_z$. In this notation, the zero-field Green function is a 4×4 matrix, the inverse of which is [14–16]

$$\hat{G}^{-1} = \begin{pmatrix} i\omega - \xi_{01} & -\epsilon_\perp & \Delta_{\mathbf{k}} & 0 \\ -\epsilon_\perp & i\omega - \xi_{02} & 0 & 0 \\ \Delta^*_{\mathbf{k}} & 0 & i\omega + \xi_{01} & \epsilon_\perp \\ 0 & 0 & \epsilon_\perp & \omega + \xi_{02} \end{pmatrix}, \tag{8}$$

where $\xi_{0n} = (\mathbf{k}^2 - k_{F\|}^2)/2m_n$ and $\epsilon_\perp = [J_1^2 + J_2^2 + 2J_1J_2\cos k_z s]^{1/2}$.

The London penetration depth is obtained from the current-current correlation function in zero external frequency and momentum [17]. For this model, the dc conductivity tensor is diagonal, with elements

$$\sigma_{xx} = 2e^2T\sum_\omega\int\frac{d^3k}{(2\pi)^3}\sum_{n,n'=1}^{2} v_{xn}v_{xn'}(G_{nn'}G_{n'n} + F_{nn'}F^\dagger_{n'n}), \tag{9}$$

$$\sigma_{zz} = 2e^2T\sum_\omega\int\frac{d^3k}{(2\pi)^3}v_z^2 \times\sum_{n\ne n'}(G_{nn}G_{n'n'} + F_{nn}F^\dagger_{n'n'} + G_{nn'}G_{nn'} + F_{nn'}F^\dagger_{nn'}), \tag{10}$$

and σ_{yy} is analogous to σ_{xx}, where all of the $G_{nn'}$ and $F_{nn'}$ are functions of k, ω, and $v_{xn} = k_{F\|}\cos\theta_{\mathbf{k}}/m_n$ and $v_z = d\epsilon_\perp/dk_z$ are the Fermi velocities along $\hat{\mathbf{x}}$ within the nth layers and normal to the layers, respectively.

It is straightforward to obtain the exact forms for the $G_{nn'}$ and $F_{nn'}$. Letting $\int d^3k = 2\pi N_1(0)\int d\xi_{01}\int_{-\pi}^{\pi}d\theta_{\mathbf{k}}\int_{-\pi}^{\pi}d\eta$, where $\xi_{02} = \beta\xi_{01}$, $\eta = k_z s$, and $N_n(0) = m_n/2\pi s$ is the single spin density of states at E_F in the nth layer, we can integrate Eqs. (7), (9), and (10) over ξ_{01} exactly. Since $\sin^2\theta_{\mathbf{k}} = \frac{1}{2}(1 - \cos2\theta_{\mathbf{k}})$, etc., integration over $\theta_{\mathbf{k}}$ leads to $\sigma_{xx} = \sigma_{yy} \equiv \sigma_{ab}$ and $\sigma_{zz} \equiv \sigma_c$ for both the s-wave and $d_{x^2-y^2}$ cases. We obtain

$$\sigma_{ab} = C_\| T\sum_{|\omega|\le\omega_\|}\int_{-\pi}^{\pi}\frac{d\eta}{2\pi}\int_{-\pi}^{\pi}\frac{d\theta_{\mathbf{k}}}{2\pi}|\Delta_{\mathbf{k}}|^2\left[\frac{(\omega^2 - \beta\epsilon_\perp^2)^2}{\alpha R^3} + \frac{\beta\omega^2}{\alpha R^2} + \frac{2\beta^3\epsilon_\perp^2(R + \omega^2 + \epsilon_\perp^2)}{\alpha^3R^2}\right], \tag{11}$$

$$\sigma_c = C_\perp J_1J_2T\sum_{|\omega|\le\omega_\|}\int_{-\pi}^{\pi}\frac{d\eta}{2\pi}\int_{-\pi}^{\pi}\frac{d\theta_{\mathbf{k}}}{2\pi}\frac{\sin^2\eta|\Delta_{\mathbf{k}}|^2}{\epsilon_\perp^2\alpha^3R}\left[\frac{\omega^2(\alpha^2 + 4\beta\epsilon_\perp^2)}{R + \omega^2 + \epsilon_\perp^2} + 2\beta^2\epsilon_\perp^2\right], \tag{12}$$

$$\Delta_{\mathbf{k}'} = \pi N_1(0)T\sum_{|\omega|\le\omega_\|}\int_{-\pi}^{\pi}\frac{d\eta}{2\pi}\int_{-\pi}^{\pi}\frac{d\theta_{\mathbf{k}}}{2\pi}\lambda_{\mathbf{k},\mathbf{k}'}\frac{\Delta_{\mathbf{k}}(\beta R + \omega^2)}{\alpha R}, \tag{13}$$

$$R = [(\omega^2 + \epsilon_\perp^2)^2 + \omega^2|\Delta_{\mathbf{k}}|^2]^{1/2}, \tag{14}$$

$$\alpha = [(1 + \beta^2)\omega^2 + \beta^2|\Delta_{\mathbf{k}}|^2 + 2\beta(R - \epsilon_\perp^2)]^{1/2}, \tag{15}$$

$C_\perp = 2\pi N_1(0)(es)^2 J_1 J_2$, $C_\parallel = \pi e^2 N/m_1$, and $N = k_{F\parallel}^2/2\pi s$ is one-half the total number of quasiparticles per unit cell. The Matsubara sums and η integrations must be performed numerically, as must the d-wave $\theta_{\mathbf{k}}$ integrations. The penetration depths $\lambda_{ii}(T) = [4\pi/\sigma_{ii}(T)]^{1/2}$, as in [17]. The bare T_c value, T_{c0}, is given by setting $\Delta_{\mathbf{k}} = 0$ and $\epsilon_\perp \to 0$ in Eq. (13). For finite $\epsilon_\perp$, $T_c < T_{c0}$, as shown for $\beta = 5$ in Fig. 1. With the forms of $\lambda_{\mathbf{k},\mathbf{k}'}$ used, both T_{c0} and T_c are identical for the s-wave and d-wave models. Equations (11)–(15) are *exact* within the standard BCS mean-field approximation.

The density of states (DOS) is found as in [15]

$$N_S(\Omega) = \frac{1}{\pi}\sum_{n=1}^{2}\int \frac{d^3k}{(2\pi)^3}\,\mathrm{Im}G_{nn}(k,\omega)\Big|_{\omega\to -i\Omega+\delta}, \quad (16)$$

where $\delta = 0+$. It is straightforward to evaluate the integral over ξ_{01} exactly, and to make the analytic continuation [15]. For the s-wave case, the $\theta_{\mathbf{k}}$ integral is trivial. A resulting s-wave plot of $N_S(\Omega)/N_1(0)$ vs Ω/T_{c0} is shown in the inset of Fig. 1. For the d-wave case (not pictured), $N_S(\Omega)$ is always linear in $|\Omega|$ for small $|\Omega|$.

In the limit $\epsilon_\perp \to 0$, the d-wave $\Delta_d(T)$ and σ_{ab} reduce to the clean limit d-wave forms of [3], and the s-wave $\Delta_s(T)$ and σ_{ab} reduce to the standard BCS forms. However, for both the s- and d-wave cases, σ_c in Eq. (12) does not reduce to these forms, since it explicitly contains hopping to the N layers. We have thus also calculated the conductivity $\tilde{\sigma}_{ii}$ for a layered superconductor with only one (S) layer per unit cell, with interlayer hopping matrix element $J = J_1 = J_2$ and c-axis band dispersion $2J\cos k_z s$ [18],

$$\tilde{\sigma}_{ii}(T) \longrightarrow \tilde{C}_i T \sum_{|\omega|\le\omega_\parallel}\int_{-\pi}^{\pi}\frac{d\theta_{\mathbf{k}}}{2\pi}\frac{|\Delta_{\mathbf{k}}|^2}{[\omega^2+|\Delta_{\mathbf{k}}|^2]^{3/2}}, \quad (17)$$

where $\tilde{C}_x = \tilde{C}_y = \tilde{N}e^2\pi/m_1$, $\tilde{C}_z = 4\pi N_1(0)e^2J^2s^2$, and $\tilde{N} = k_{F\parallel}^2/2\pi s$ is the total number of quasiparticles per unit cell. In the limit $J_1 = J_2 \to J$ and $s \to 2s$, $N \to \tilde{N}/2$, $C_\perp \to \tilde{C}_z$, and $C_\parallel \to \tilde{C}_x/2 = \tilde{C}_y/2$, as expected. Clearly, for both OPs, one obtains the BCS or standard d-wave T-dependence for all field directions, with a constant anisotropy ratio $\tilde{\sigma}_{xx}/\tilde{\sigma}_{zz} = \tilde{C}_x/\tilde{C}_z$. We note that this d-wave $\sigma_c(T)$ differs substantially from that obtained with a spherical Fermi surface [19].

Measurements of $\lambda_{ab}(0)$ in single crystal YBCO have been made by a variety of techniques. Among these, high-field muon spin rotation [20,21], low-field rf [22], and low-field dc magnetization measurements [23] all gave $\lambda_{ab}(0)$ results consistent with 1400 ± 100 Å. Hence, this range of values does not depend substantially upon the measurement techniques, fields, and frequencies used.

In Fig. 2, we have presented the microwave cavity YBCO $\lambda_{ab}(T)$ data of Bonn *et al.* [24], which is very similar to that of [7]. We have normalized the data relative to that at the lowest measurement temperature $T_0 = 1.35$ K. The data (solid diamonds) are presented as $\lambda_{ab}^2(T_0)/\lambda_{ab}^2(T)$ vs T/T_c for $\lambda_{ab}(T_0) = 1400$ Å. Also shown are the YBCO data (triangles) of Yethiraj *et al.* [25] obtained from neutron scattering of the vortex lattice with $\mathbf{H} \parallel \hat{\mathbf{c}}$ above $H_{c1,\perp}$. Since the lowest T in that data set was 11 K, for comparison the raw intensity data [proportional to $\sigma_{ab}^2(T)$] was adjusted by extrapolating the linear, low-T regime to T_0, and then taking the square root. Also shown in Fig. 2 are the predictions of our best low-T fits (s-wave: $\beta = 5$, $J_1/T_{c0} = 3$, $J_c/T_{c0} = 2.6$, solid curve; d-wave: $\beta = 5$, $J_1/T_{c0} = J_2/T_{c0} = 9$, dashed curve) for $\lambda_{ab}(T_0) = 1400$ Å, and the standard d-wave model [Eq. (17)] (dotted curve). Varying the choice of $\lambda_{ab}(T_0)$ from 1300 to 1500 Å causes comparable changes in the fitting parameters J_1 and J_2. It is readily seen that the data of [24] and [25] are consistent. The details of our fits to the low-T region are shown in the inset of Fig. 2. The (adjusted) data of [25] are also shown. These two low-T points correspond to a best choice of $\lambda_{ab}(T_0) \approx 1600$ Å, as claimed from 11 K absolute intensity measurements in [25]. The s-wave choice of parameters $\beta = 5$, $J_1/T_{c0} = 3.4$, and $J_2/T_{c0} = 3.0$ fits

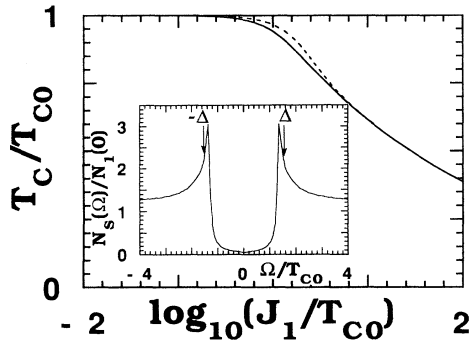

FIG. 1. Plots of T_c/T_{c0} vs $\log_{10}(J_1/T_{c0})$ for $\beta = 5$, $\lambda_0 N_1(0) = 0.1$, $J_2/J_1 = 1$ (solid) and 0.1 (dashed). Inset: Plot of $T = 0$ s-wave $N_S(\omega)/N_1(0)$ vs ω/T_{c0} for $\beta = 5$, $J_1/T_{c0} = 3$, $J_2/T_{c0} = 2.6$. ↓: $\pm\Delta(0)$, $\Delta(0) \approx 1.558T_{c0} \approx 1.967T_c$.

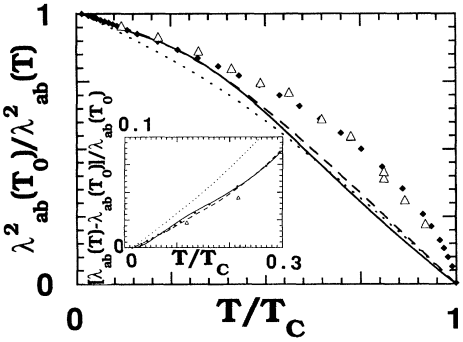

FIG. 2. Plots of $\lambda_{ab}^2(T_0)/\lambda_{ab}^2(T)$ vs T/T_c. ◆: data from [24] with $\lambda_{ab}(T_0) = 1400$ Å, $T_0 = 1.35$ K $= 0.0145T_c$. △: data from [25]. Solid: s-wave model with $\beta = 5$, $J_1/T_{c0} = 3$, $J_2/T_{c0} = 2.6$. Dashed: d-wave model with $\beta = 5$, $J_1/T_{c0} = J_2/T_{c0} = 9$. Dotted: standard d-wave model. Inset: Low-T region of $[\lambda_{ab}(T) - \lambda_{ab}(T_0)]/\lambda_{ab}(T_0)$ vs T/T_c.

these two low-T data points quite well. The standard d-wave curve could be made consistent with the data by allowing for strong coupling effects [19].

While the fits in the low-T regime of our theory with both OPs to the data of [24,25] are excellent, the fits in the vicinity of T_c are poor. Such discrepancies could arise from either strong coupling effects or from critical fluctuations [26].

Since the fitted s-wave and d-wave $\lambda_{ab}(T)$ curves are rather similar, it would be most interesting to compare the corresponding predicted curves for $\lambda_c(T)$. In Fig. 3, we have plotted $\lambda_c^2(T_0)/\lambda_c^2(T)$ for the same s- and d-wave parameter choices used in Fig. 2, along with the standard d-wave model. The details of the low-T behaviors are plotted in the inset as $[\lambda_c(T) - \lambda_c(T_0)]/\lambda_c(T_0)$, for $T_0 = 0.145T_c$, as in Fig. 2. The predictions for $\lambda_c(T)$ are *strikingly* different. We conclude that while measurements of $\lambda_{ab}(T)$ alone cannot conclusively distinguish between the various models, measurements of both $\lambda_{ab}(T)$ and $\lambda_c(T)$ on the same sample should be much better at distinguishing between the models.

Neutron scattering data involving $\lambda_c(T)$ were also obtained in [25]. At general θ, T, the scattering intensity is proportional to $\sigma_{ab}(T)[\sigma_{ab}(T)\cos^2\theta + \sigma_c(T)\sin^2\theta]$. Using the experimental θ and $\Gamma(0) \equiv \lambda_c(0)/\lambda_{ab}(0)$ values [25], neither the s- nor the d-wave fits predicted any observable difference in the T dependence of the scattering intensity, consistent with the rather large error bars in the data of [25]. However, neutron scattering at field angles much closer to parallel to the layers *should* be able to discriminate between these theories. Also, microwave cavity measurements of both $\lambda_c(T)$ and $\lambda_{ab}(T)$ are possible, but have not yet been published. We propose these measurements as a new test for the orbital symmetry of the superconducting order parameter, or at least as a test of the relative importance of the N layers.

Finally, we note that the DOS curve (in the inset of Fig. 1) of our s-wave fit is different from that of the standard d-wave model, even though the predicted $\lambda_{ab}(T)$ are very similar. Our s-wave DOS is nearly gapless, with a quasilinear energy dependence, and a slope that is less than that for the standard d-wave model. However, the penetration depth is *not* simply related to the DOS, *except* in single layer models. For two layers per unit cell, there are additional terms in $\lambda_{ab}(T)$, arising from the $G_{12}G_{21}$ and $F_{12}F_{21}^{\dagger}$ terms in Eq. (9).

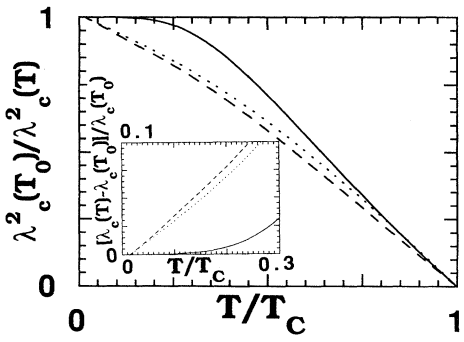

FIG. 3. Plots of $\lambda_c^2(T_0)/\lambda_c^2(T)$ vs T/T_c for the same models and parameters as in Fig. 2. Inset: Low-T region of $[\lambda_c(T) - \lambda_c(T_0)]/\lambda_c(T_0)$ vs T/T_c.

The authors would like to thank D. Bonn and M. Yethiraj for supplying their data electronically. They would also like to thank A. A. Abrikosov, M. R. Beasley, D. Bonn, W. N. Hardy, M. Ledvij, T. Timusk, M. Yethiraj, and Y. Zha for useful discussions. This work was supported by the U.S. Department of Energy, Division of Basic Energy Sciences, under Contracts No. W-31-109-ENG-38 and No. DE-AC005-84OR21400 with Martin Marietta Energy Systems, Inc.

[1] Z.-X. Shen *et al.*, Phys. Rev. Lett. **70**, 1553 (1993).
[2] D. A. Wollman *et al.*, Phys. Rev. Lett. **72**, 2134 (1994).
[3] P. J. Hirschfeld and N. Goldenfeld, Phys. Rev. B **48**, 4219 (1993).
[4] A. G. Sun *et al.*, Phys. Rev. Lett. **72**, 2267 (1994).
[5] P. Chaudhari and S.-Y. Lin, Phys. Rev. Lett. **72**, 1084 (1994).
[6] J. Buan *et al.*, Phys. Rev. Lett. **72**, 2632 (1994).
[7] W. N. Hardy *et al.*, Phys. Rev. Lett. **70**, 3999 (1993).
[8] N. Klein *et al.*, Phys. Rev. Lett. **71**, 3355 (1993).
[9] Z. Ma *et al.*, Phys. Rev. Lett. **71**, 781 (1993).
[10] S. Anlage *et al.*, Phys. Rev. B **44**, 9764 (1991).
[11] D. H. Wu *et al.*, Phys. Rev. Lett. **70**, 85 (1993).
[12] R. A. Klemm *et al.*, Phys. Rev. Lett. **73**, 1871 (1994).
[13] S. H. Liu and R. A. Klemm, Phys. Rev. Lett. **73**, 1019 (1994).
[14] A. A. Abrikosov and R. A. Klemm, Physica (Amsterdam) **191C**, 224 (1992).
[15] R. A. Klemm and S. H. Liu, Physica (Amsterdam) **191C**, 383 (1992); Phys. Rev. B **48**, 4080 (1993); **48**, 10650 (1993).
[16] L. N. Bulaevskiĭ and M. V. Zyskin, Phys. Rev. B **42**, 10230 (1990).
[17] A. A. Abrikosov, L. P. Gor'kov, and I. E. Dzyaloshinskiĭ, *Methods of Quantum Field Theory in Statistical Physics* (Prentice-Hall, Inc., Englewood Cliffs, 1963), Sec. 37.1.
[18] C. Jiang and J. P. Carbotte, Phys. Rev. B **45**, 10670 (1992).
[19] M. Prohammer and J. P. Carbotte, Phys. Rev. B **43**, 5370 (1991).
[20] D. R. Harshman *et al.*, Phys. Rev. B **39**, 851 (1989).
[21] J. E. Sonier *et al.*, Phys. Rev. Lett. **72**, 744 (1994).
[22] S. Sridhar *et al.*, Phys. Rev. Lett. **63**, 1873 (1989).
[23] L. Krusin-Elbaum *et al.*, Phys. Rev. Lett. **62**, 217 (1989).
[24] D. A. Bonn *et al.*, Phys. Rev. B **50**, 4051 (1994).
[25] M. Yethiraj *et al.*, Phys. Rev. Lett. **71**, 3019 (1993).
[26] S. Kamal *et al.*, Phys. Rev. Lett. **73**, 1845 (1994).